

NONLINEAR OPTICAL PHENOMENA

PACS numbers: 42.68.Ay; 42.65.Re; 33.80.Eh
DOI: 10.1070/QE2008v038n12ABEH013860

Peculiarities of the spatial focusing of a high-power femtosecond laser pulse in air

Yu.E. Geints, A.A. Zemlyanov

***Abstract*. The propagation of focused high-power femtosecond laser pulses in air is numerically simulated. The dependences of the effective average size of a focal spot and the maximum achievable radiation intensity in the focal beam waist on the peak power of incident radiation are studied. It is shown that in the regime of nonstationary self-action of radiation, due to photoionisation of the medium and formation of plasma, it becomes impossible to focus radiation into a spot of diffraction-limited size predicted by a linear theory.**

Keywords: *femtosecond laser radiation, focal beam waist, nonstationary self-focusing, photoionisation of a medium.*

1. Introduction

The achievement of nearly diffraction-limited focal light beam waists and high radiation intensities is very important in many scientific and technological fields. This is required, for example, for manufacturing multilayer optical structures in dielectrics with the help of laser beams [1], in laser cell microsurgery [2], laser scanning microscopy of living tissues [3], and laser metal and ceramics machining [4]. The use of high-power femtosecond laser pulses in such technologies can provide very high radiation intensities in the focal laser beam waist at pulse energies of only a few millijoules [5]. The advantages of irradiation of targets by ultrashort laser pulses are the low energy thresholds for ionisation and ablation of materials compared to those typical for irradiation by longer radiation pulses as well as minimal thermal and mechanical damages of the regions adjacent to the irradiated region of a sample. In addition, the study of the properties of focusing of high-power femtosecond laser pulses in air is also of considerable interest for describing the propagation of these pulses over long atmospheric paths [6].

The high peak power and intensity of femtosecond pulses can violate the linear regime of their focusing even before they reach a target. The Kerr self-focusing of radiation in gases and condensed media, multiphoton absorption, plasma production in media, and a number of other nonlinear effects cause nonlinear changes in the optical properties of media. In this case, the linear theory of diffraction of electromagnetic radiation, which gives certain relations between the numerical aperture of a focused light beam and the size of its focal spot, cannot be applied even for preliminary estimates of parameters of high-power ultrashort pulses in the region of their focusing.

In this paper, we simulated numerically the formation of the spatial structure of a tightly focused high-power femtosecond beam in the focal waist under conditions of nonstationary self-action. The main attention was devoted to the study of the dependences of the effective size of the focal beam waist and the maximum achievable radiation intensity on the power of a femtosecond laser beam focused in air.

Yu.E. Geints, A.A. Zemlyanov Institute of Atmospheric Optics, Siberian Branch, Russian Academy of Sciences, prosp. Akademicheskii 1, 634005 Tomsk, Russia; e-mail: ygeints@iao.ru, zaa@iao.ru

Received 4 April 2008
Kvantovaya Elektronika **38** (12) 1127 – 1134 (2008)
Translated by M.N. Sapozhnikov

2. Linear and nonlinear laser radiation focusing

The focal waist radius R_f of a laser beam with the Gaussian envelope $E(\boldsymbol{r}_\perp, z)$

$$E(\boldsymbol{r}_\perp, z=0) = E_0 \exp\left[-\frac{|\boldsymbol{r}_\perp|^2}{2R_0^2} + i\varphi_f(\boldsymbol{r}_\perp)\right] \quad (1)$$

of the electric field propagating linearly in a medium with the refractive index n_0 is described by the expression

$$R_f = R_0 \frac{F_0}{(F_0^2 + k_0^2 R_0^4)^{1/2}} = R_0 \frac{1}{(1 + 4/\bar{F}_0^2)^{1/2}}. \quad (2)$$

Here, $|\boldsymbol{r}_\perp| = (x^2 + y^2)^{1/2}$ is the transverse coordinate; E_0 is the wave amplitude; $\varphi_f = -k_0(|\boldsymbol{r}_\perp|^2/F_0)$ is the wave phase acquired due to the initial beam focusing; R_0 is the initial radius of the beam; F_0 is the radius of initial curvature of the wave phase front; $k_0 = 2\pi n_0/\lambda_0$ is the wave number; and λ_0 is the wavelength in vacuum. The beam waist itself has a centre located at a point with coordinate $\bar{z}_f = 4\bar{F}_0/(\bar{F}_0^2 + 4)$ (linear focus) and the characteristic length $\bar{L}_f = 4(R_f/R_0)^2$. Hereafter, the dimensional quantities are normalised for convenience to the Rayleigh length $L_R = k_0 R_0^2/2$ and are denoted by a bar at the top.

The focal waist radius is inherently restricted by the radiation wavelength λ_0, which gives, according to (2), the minimal radius of a focal spot $R_f^* \simeq \lambda_0/2$ [7].

Upon laser beam focusing, the radiation intensity averaged over the focal spot area $I_f^{av} = P_0/(\pi R_f^2)$ (where $P_0 = [cn_0/(8\pi)] \int |E|^2 d\boldsymbol{r}_\perp$ is the incident radiation power)

increases with respect to the incident intensity $I_0^{\rm av} = P_0/(\pi R_0^2)$ proportionally to the square of the inverse diffraction angular divergence $\theta_{\rm d}$:

$$\mu_{\rm f} = \frac{I_{\rm f}^{\rm av}}{I_0^{\rm av}} = 1 + \frac{R_0^2}{F_0^2\theta_{\rm d}^2}, \quad \theta_{\rm d} = \frac{1}{k_0 R_0}. \tag{3}$$

A light beam propagating in a medium with the Kerr nonlinearity experiences self-action. The refractive index n of such a medium becomes a function of the optical field intensity I: $n(I) = n_0 + n_2 I$ (where the parameter n_2 characterises the optical power of the Kerr effect), which results in the self-focusing of the light wave. According to the approximate theory of stationary self-focusing [8], if the beam power exceeds the critical power $P_{\rm cr}$, the beam will experience a transverse collapse due to the Kerr effect (contracts to a point) over the distance $\bar{z}_{\rm K} = 1/(\eta - 1)^{1/2}$, where $\eta = P_0/P_{\rm cr}$, $P_{\rm cr} = \lambda_0^2/(2\pi n_2)$. Obviously, for $\eta = 1$ in the case of a collimated beam, a nonlinear Kerr lens compensates the natural spread of the beam.

From the point of view of linear optics, the Kerr effect is equivalent to the focusing of a light beam by a spherical lens with the focal length depending on the radiation power. If the laser beam was initially focused to a point $z = z_{\rm f}$ and propagated in the Kerr medium, the position $z_{\rm n}$ of the nonlinear focus of the beam will be determined taking into account the combined action of the initial and induced focusing:

$$z_{\rm n} = z_{\rm K} F_0/(z_{\rm K} + F_0). \tag{4}$$

The beam focusing parameters in the Kerr medium estimated from expressions of the approximate theory of stationary self-focusing [8] show that the laser beam can be focused into a spot of size that is even smaller than the diffraction limit, which could provide extremely high optical field intensities in an extremely small volume [9]. However, this effect is not observed in real situations because of physical mechanisms preventing the further self-compression of the laser beam, which are always realised at high radiation intensities. The most important of them in gases and condensed media are ionisation and the production of plasma in the laser beam.

The Drude–Lorentz model [10] of a free electron gas gives the expression for the change in the complex refractive index $m = n + {\rm i}\varkappa$ of a medium caused by photoionisation:

$$m_{\rm p} = m - n_0 = -\frac{\omega_{\rm p}^2\tau_{\rm c}^2}{2n_0(\omega^2\tau_{\rm c}^2 + 1)}\left(1 - \frac{\rm i}{\omega\tau_{\rm c}}\right), \tag{5}$$

where $\omega_{\rm p} = [e^2\rho_{\rm e}/(m_{\rm e}\varepsilon_0)]^{1/2}$ is the plasma frequency; $\rho_{\rm e}$ is the free electron concentration (plasma density); $\tau_{\rm c}$ is the characteristic time of collisions of free electrons with heavy particles; e and $m_{\rm e}$ is the electron charge and mass; ω is the light-wave frequency; and $\varepsilon_0 = 8.8 \times 10^{-12}$ F m^{-1} is the universal electric constant. One can see from expression (5) that the influence of the plasma nonlinearity on the optical field is manifested in the change in the wave phase (the real part of $m_{\rm p}$), resulting in the wave defocusing, and in the decrease in the field energy (the imaginary part of $m_{\rm p}$) due to absorption of photons by free ions. In this case, the parameter $|m_{\rm p}|$ is proportional to the instant electron density $\rho_{\rm e}$.

The instant free electron density in a medium can be determined from the rate equation taking into account the multiphoton and cascade ionisation mechanisms, as well as a decrease in the electron concentration due to their recombination with ions:

$$\frac{\partial\rho_{\rm e}}{\partial t} = W_{\rm i}(I)(\rho_{\rm nt} - \rho_{\rm e}) + \frac{\sigma_{\rm c}}{n_0\Delta E_{\rm i}}\rho_{\rm e} I - v_{\rm r}\rho_{\rm e}^2, \tag{6}$$

where $W_{\rm i}(I)$ is the rate of photoionisation of the medium depending on the light-wave intensity; $\rho_{\rm nt}$ is the density of neutral atoms (molecules); $\sigma_{\rm c} = \omega_{\rm p}^2\tau_{\rm c}/[c\rho_{\rm e}(\omega^2\tau_{\rm c}^2 + 1)]$ and $\Delta E_{\rm i}$ are the cascade ionisation cross section and ionisation potential of molecules, respectively; and $v_{\rm r}$ is the recombination rate. In the case of high-power femtosecond laser pulses propagating in gas, the two last terms in the right-hand side of Eqn (6) prove to be insignificant compared to the first one and, therefore, they are neglected, as a rule, in estimates of the plasma density.

The photoionisation of molecules gives rise to the additional absorption of radiation in the medium. The corresponding nonlinear absorption coefficient $\alpha_{\rm i}$ of the medium is described by the expression

$$\alpha_{\rm i} = \frac{W_{\rm i}(i)}{I}\Delta E_{\rm i}(\rho_{\rm nt} - \rho_{\rm e}).$$

Thus, the total absorption coefficient of the wave energy during the plasma formation in air has the form

$$\alpha_{\rm n} = \alpha_{\rm p} + \alpha_{\rm i} = \sigma_{\rm c}\rho_{\rm e} + \frac{W_{\rm i}(I)}{I}\Delta E_{\rm i}(\rho_{\rm nt} - \rho_{\rm e}), \tag{7}$$

where $\alpha_{\rm p} = k_0 {\rm Im}\, m_{\rm p}$. The absorption of radiation reduces the instantaneous pulse intensity, thereby decreasing the focusing effect of the Kerr nonlinearity.

Note that at high radiation intensities the hyperpolarisability of the medium related to the fifth-order nonlinear susceptibility $\chi^{(5)}$ can be manifested. In this case, the refractive index can be written as a sum of three terms: $n(I) = n_0 + n_2 I - n_4 I^2$. One can see that the nonlinear addition n_4 reduces the focusing action of the Kerr effect due to saturation: $n_2(I) = n_2 - n_4 I \simeq n_2/(1 + I/I_{\rm sat})$, where $I_{\rm sat} = n_2/n_4$ is the characteristic saturation intensity [11]. It is obvious that the specific role of the fifth-order nonlinearity during the self-focusing of radiation will be determined by the relation between the characteristic saturation and plasma-formation intensities, which in turn depend on the optical parameters of the medium itself. For example, for the atmospheric air at the wavelength $\lambda_0 = 800$ nm, we have $n_2 = 3.2 \times 10^{-19}$ cm^2 W^{-1}, $n_4 = 2.5 \times 10^{-33}$ cm^4 W^{-2} [12], and the saturation intensity is $I_{\rm sat} = 10^{14}$ W cm^{-2}. In this case, the active plasma formation in air, as show numerous theoretical calculations (see review [13]), begins already at pulse intensities $I \sim 10^{13}$ W cm^{-2}, which allows us to neglect the hyperpolarisability of the medium in further calculations.

3. Numerical model of radiation propagation

We simulated the focusing of ultrashort laser pulses in gases by using the nonlinear Schrödinger equation (NSE) written for the slowly varying complex amplitude of the electromagnetic field of a light pulse $U(\boldsymbol{r}, z, t) = E/E_0$. This

equation takes into account, along with the beam diffraction and frequency dispersion of air, a number of nonlinear effects responsible for the amplitude and phase self-modulation of the light wave (see, for example, [14]). Let us write the NSE in the form

$$\left(\frac{\partial}{\partial z}-\frac{\mathrm{i}}{2n_0k_0}\nabla_\perp^2+\frac{\mathrm{i}}{2}\frac{\partial^2 k}{\partial\omega^2}\frac{\partial^2}{\partial t^2}\right)U(\boldsymbol{r}_\perp,z,t)$$

$$-\mathrm{i}k_0(\tilde{n}_2-n_\mathrm{p})U(\boldsymbol{r}_\perp,z,t)+\frac{\alpha_\mathrm{n}}{2}U(\boldsymbol{r}_\perp,z,t)=0. \qquad (8)$$

Here, $n_\mathrm{p}=\mathrm{Re}\,m_\mathrm{p}$; $\partial^2k/\partial\omega^2=0.21$ fs^2 cm^{-1} in air for $\lambda_0=800$ nm;

$$\tilde{n}_2=\frac{n_2}{2}\left[(1-\beta)|U|^2+\beta\int_{-\infty}^{t}\mathrm{d}t'\Lambda(t-t')|U(t')|^2\right]$$

is the cubic addition to the refractive index taking into account the instant and inertial contributions to the Kerr effect; and β is the specific contribution of the inertial Kerr effect.

The inertial component $\Lambda(t)$ of the Kerr effect is related to the finite orientation time of anisotropic molecules along the electric field vector. The inertial response was taken into account in the decaying oscillator model [15]: $\Lambda(t)=\theta(t)\Omega_\mathrm{R}\exp(-t/\tau_\mathrm{d})\sin\Omega_\mathrm{R}t$, where $\Omega_\mathrm{R}\simeq 20$ THz is a vibrational molecular frequency; $\tau_\mathrm{d}\simeq 70$ ns is the decay time (in air) and $\theta(t)$ is the Heaviside function.

The numerical integration of NSE (8) was performed by the method of division of the initial problem into two subproblems at each step over the evolution variable z. In the first, nonlinear subproblem, the phase incursion of the optical wave due to nonlinear optical effects was determined, while in the second, linear subproblem, the diffraction and dispersion of a wave packet were calculated with the phase front determined at the previous step. The calculation stability was improved by combining the spectral Fourier method (in time), the implicit three-layer difference Crank–Nicholson scheme (in transverse coordinates), and the adaptive correction of a network step over the evolution variable. The free electron density ρ_e was calculated by solving Eqn (6) by the Runge–Kutta method.

4. Model of gas photoionisation

We used the Perelomov–Popov–Terent'ev model of gas photoionisation [16], which, as shown in [17], most completely describes the experimental data available at present. According to this model, the ionisation rate $W_\mathrm{i}(I)$ of a level with the bond energy ΔE_i, the orbital momentum l and its projection j to the field direction is described by the expression

$$W_\mathrm{i}(I)=\frac{\Delta E_\mathrm{i}}{\hbar}|C_{nl}|^2f_{lj}\left(\frac{6}{\pi}\right)^{1/2}\left(\frac{2E_\mathrm{a}}{E}\right)^{2n^*-3/2}(1+\gamma^2)^{3/4}$$

$$\times A_j(\gamma)\exp\left[-\frac{2E_\mathrm{a}}{3E}g(\gamma)\right], \qquad (9)$$

where $\gamma=(\omega_0/c)(c\varepsilon_0m_\mathrm{e}\Delta E_\mathrm{i}/I)^{1/2}$ is the Keldysh parameter; E_a is the intratomic field strength; $|C_\mathrm{nl}|^2=2^{4n^*-2}\times[n^*\Gamma(n^*+l+1)\Gamma(n^*-l)]^{-1}$; $n^*=Z(\Delta E_\mathrm{H}/\Delta E_\mathrm{i})^{1/2}$ is the effective principal quantum number; Z is the charge of the atomic or ion core; ΔE_H is the ionisation energy of the hydrogen atom;

$$g(\gamma)=\frac{2}{3\gamma}\left[\left(1+\frac{1}{2\gamma^2}\right)\mathrm{arcosh}\,\gamma-\frac{(1+\gamma^2)^{1/2}}{2\gamma}\right];$$

$$f_{lj}=\frac{(2l+1)(i+|j|)!}{2^{|j|}|j|!(l-|j|)!};\quad A_j(\gamma)=\frac{4}{\sqrt{3}\pi}\frac{1}{|j|!}\frac{\gamma^2}{1+\gamma^2}$$

$$\times\sum_{l\geqslant m_\mathrm{i}}^{\infty}\exp[-\alpha(l-m_\mathrm{i})]W_j\left[\beta(l-m_\mathrm{i})^{1/2}\right];$$

$$\alpha=2\left(\mathrm{arsinh}\,\gamma-\frac{\gamma}{1+\gamma^2}\right);\quad\beta=\frac{2\gamma}{(1+\gamma^2)^{1/2}};$$

$$W_j(x)=\exp(-x^2)\int_0^x\exp(-y^2)(x^2-y^2)^{|j|!}\mathrm{d}y;$$

m_i is the photoionisation order.

In practice the use of expression (9) in the numerical simulation of the NSE to calculate the ionisation rate is not always convenient because it is necessary to calculate many coefficients at each step of a change in the wave intensity. To increase the calculation rate, we used instead of the dependence $W_\mathrm{i}(I)$ (9) its approximation $W_\mathrm{i}(I)=A_W(I)I^K$, where coefficients A_W and K were selected according to the medium type and the laser wavelength. Thus, we obtained for atmospheric gases the function in the form

$$\lg[A_W(I)]=\lg A_0-A_\mathrm{i}\exp\left[-\frac{\lg^2(I/I_\mathrm{cr})}{A_2^2}\right]$$

$$=\lg A_0-A_\mathrm{i}\exp\left[-\frac{1}{A_2^2}\lg^2\left(\frac{I_0}{I_\mathrm{cr}}|U|^2\right)\right],$$

where A_W is taken in s^{-1} m^{2K} W^{-K} and I_0 and I_cr – in W m^{-2}; $K=7.44$, $\lg A_0=-119.378$, $A_1=13.445$, $A_2=2.041$, and $\lg I_\mathrm{cr}=20.616$ for oxygen O_2; $K=10.165$, $\lg A_0=-168.530$, $A_1=19.223$, $A_2=2.012$, and $\lg I_\mathrm{cr}=20.688$ for nitrogen N_2.

5. Structure of the nonlinear focus of ultrashort pulses

Consider the numerical simulation of the evolution of parameters of high-power femtosecond radiation focused in air. For definiteness, we decided to reproduce numerically experimental conditions [18] by specifying the initial shape of the normalised envelope of the radiation electric field by a Gaussian (in time and space)

$$U(\boldsymbol{r}_\perp,z,t)=\exp\left[-\frac{|\boldsymbol{r}_\perp|^2}{2R_0^2}+\mathrm{i}\varphi_\mathrm{f}(\boldsymbol{r}_\perp)-\frac{t^2}{2t_\mathrm{p}^2}\right]$$

with the following parameters: the pulse duration $t_\mathrm{p}=60$ fs, the beam radius $R_0=2.8$ mm (at the 1/e level), and the wavelength $\lambda_0=800$ nm. The initial radius of curvature of the radiation phase front is $F_0=86$ cm, so that its normalised value is $\bar{F}_0=F_0/L_\mathrm{R}=0.028$ ($L_\mathrm{R}=30.8$ m).

The initial radiation energy was specified for the cases of the subcritical radiation energy ($\eta=0.1$, $P_\mathrm{cr}=3.2$ GW cm^{-2}) and of the sevenfold excess over the critical power P_cr ($\eta=7$). The initial peak intensity was $I_0=1.3\times10^9$ and 9×10^{10} W cm^{-2} in the first and second cases, respectively. The estimate of the position (4) of the nonlinear focus of the beam for $\eta=7$ gives $z_\mathrm{K}=13$ m and

$z_n = 81$ cm, i.e. the Kerr effect under these conditions only slightly shifts the beam waist from its position in a linear medium.

Figure 1 presents the dependence of the transverse sizes of a laser beam on the longitudinal coordinate: the geometrical radius R_1 determined from the profile $w(\boldsymbol{r}_\perp, z) = \int_{-\infty}^{\infty} I(\boldsymbol{r}_\perp, z, t')\mathrm{d}t'$ of the beam energy density at the 1/e level, and the effective radius R_{eff} calculated as the normalised second-order moment of the wave intensity [15]

$$R_{\mathrm{eff}}(z) = \left[\frac{1}{W(z)}\int_{-\infty}^{\infty}\mathrm{d}t'\iint_{S_\perp}\mathrm{d}^2\boldsymbol{r}_\perp I(\boldsymbol{r}_\perp, z, t')|(\boldsymbol{r}_\perp - \boldsymbol{r}_{\mathrm{gr}})|^2\right]^{1/2}, \quad (10)$$

where $\boldsymbol{r}_{\mathrm{gr}} = W^{-1}(z)\int_{-\infty}^{\infty}\mathrm{d}t'\iint_{S_\perp}\boldsymbol{r}_\perp I(\boldsymbol{r}_\perp, z, t')\mathrm{d}^2\boldsymbol{r}_\perp$ is the radius vector of the centre of gravity of the beam; W is the total energy of the radiation pulse; and $S_\perp$ is the integration region over the beam cross section. Note that the parameter R_{eff} is useful for analysis of complicated beam intensity profiles because, according to its definition, it gives the size of a spatial region in which no less than 50 % of the total beam energy is contained. In the case of a Gaussian transverse intensity profile, the geometrical and effective radii are identical.

One can see from Fig. 1 that the propagation of a focused beam in linear and nonlinear regimes occurs differently. For $\eta = 7$, a noticeable difference between R_1 and R_{eff} is observed beginning already from $z = 40$ cm. Then, an extended axial structure – a light filament, is formed in the focal beam waist ($z \geqslant 80$ cm). The difference between R_1 and R_{eff} is caused by influence of the Kerr nonlinearity which causes the sharpening of the initially Gaussian beam, thereby decreasing its geometrical size; however, no considerable redistribution of the pulse energy over the bean cross section occurs.

The evolution of the effective radius R_{eff}, unlike the evolution of its geometrical radius R_1 during the focusing of a supercritical-power beam, leads to the formation of a distinct focal beam waist centred at $z_g \simeq 84$ cm. It is important to note that the change in the effective radius of a tightly focused beam along the path in linear and nonlinear regimes occurs similarly up to the 'global' nonlinear focus for $z = z_g$, which is formed during self-focusing earlier than the geometrical focus: $z_g < z_f$.

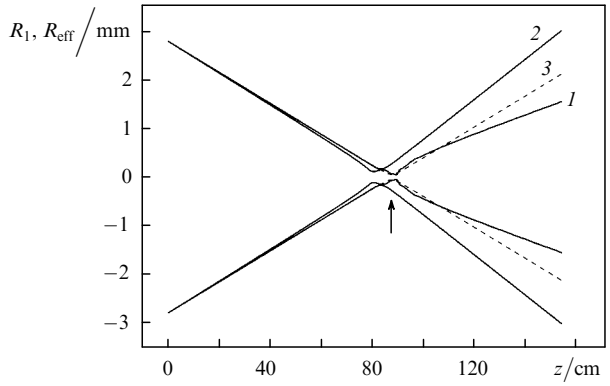

Figure 1. Geometrical (*1*, *3*) and effective (*2*) radii of tightly focused femtosecond beams as functions of the longitudinal coordinate for relative initial pulse powers $\eta = 7$ (*1*, *2*) and 0.1 (*3*). The vertical arrow indicates the position of the geometrical focus.

The first minimum of the dependence $R_1(z)$ appears at the 'local' nonlinear focus $z = z_n$; in this case, $R_1(z_n) \simeq 114$ μm, which is almost three times greater than the radius of the focal beam waist $R_f = 43$ μm during linear propagation. This is explained by the ionisation of air and plasma production, which stop the further compression of the beam by forming together with the Kerr effect a light filament on the axis with the quasi-constant peak intensity $I_{\max} \approx 4 \times 10^{13}$ W cm^{-2}. However, the transverse size of this structure is not constant but oscillates along the path, achieving the absolute minimum $R_1 \simeq R_f$ at the point $z \simeq 89$ cm, and then the beam begins to diverge monotonically.

Consider the stages of formation of a nonlinear focal waist of ultrashort pulses in more detail. For this purpose, we introduce another dimensional parameter of the beam – the instant effective radius R_{eff} whose square is described by the expression

$$R^2_{\mathrm{eff}\,t}(z,t) = P^{-1}(z,t)\iint_{S_\perp}\mathrm{d}^2\boldsymbol{r}_\perp I(\boldsymbol{r}_\perp, z, t')|(\boldsymbol{r}_\perp - \boldsymbol{r}_{\mathrm{gr}\,t})|^2 \quad (11)$$

where $\boldsymbol{r}_{\mathrm{gr}\,t} = P^{-1}(t,z)\int\int_{S_\perp}\boldsymbol{r}_\perp I(\boldsymbol{r}_\perp, z, t')d^2\boldsymbol{r}_\perp$. One can see that this parameter determines the effective size of the beam in each individual time 'slice' and is related to the time-integrated effective radius (10) by the obvious expression

$$R^2_{\mathrm{eff}}(z) = \left[\int_{-\infty}^{\infty}P(z,t)\mathrm{d}t\right]^{-1}\int_{-\infty}^{\infty}P(z,t)R^2_{\mathrm{eff}\,t}(z,t)\mathrm{d}t. \quad (12)$$

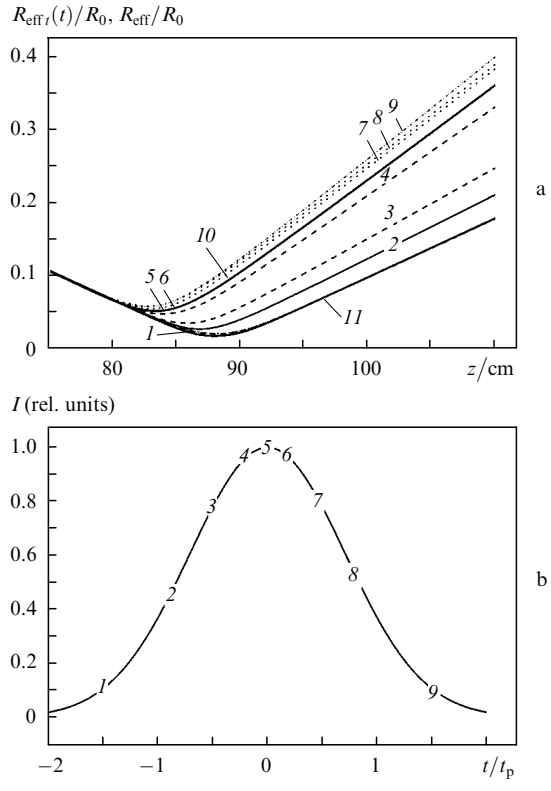

Figure 2. Evolution of the instant effective radius $R_{\mathrm{eff}\,t}$ (*1*–*9*) and integrated effective radius R_{eff} (*10*) of a focused femtosecond beam with the initial power $\eta = 7$ (a) and the time profile of the relative pulse intensity (b). The numbers of curves (*1*–*9*) in Fig. 2a correspond to the temporal slices of the pulse indicated by the numbers in Fig. 2b. Curve (*11*) corresponds to the beam radius in the linear focusing regime.

The variation of $R_{\mathrm{eff}\,t}$ along the path is shown in Fig. 2a. Curves (*1–9*) correspond to different instants of time with the light pulse duration, which are numbered in the curve presented in Fig. 2b. Thus, curves (*1–3*) describe the change in the effective radius for the leading edge of the pulse, curves (*7–9*) describe this change for the trailing edge, while curves (*4–6*) describe this change for the central part of the laser pulse. Figure 2a also shows the dependences of the integrated effective radius $R_{\mathrm{eff}}(z)$ for linear and nonlinear near propagations of the beam.

One can see from Fig. 2 that all the time 'slices' of the pulse up to a certain point of the path ($z \simeq z_{\mathrm{n}}$) evolve in the same way, and then each of them forms a focal waist whose position $z_{\mathrm{f}\,t}$ and radius $R_{\mathrm{eff}\,t\mathrm{f}} = R_{\mathrm{eff}\,t}(z_{\mathrm{f}\,t})$ depend on the position of each section within the pulse. The pulse power in the leading edge of the pulse [curve (*1*)] is lower than the critical value, the nonlinearity of the medium is not induced in fact and the spatial radius changes as in the linear case [curve (*11*)]. The higher power (compared to P_{cr}) corresponding to the time slice [curves (*2–4*)], the stronger influence of the Kerr self-focusing on the time slice. Because upon gas photoionisation the free electron density at each point of the path increases with time [see Eqn (6)], the successive slices of the pulse will be subjected to a stronger compensation by the plasma nonlinearity. This leads to the increase in the focal waist size in each next time slice and draws its centre nearer the path onset. As a result, instead of one focal spot, known in linear optics, a long waist with a variable diameter is formed upon focusing of high-power femtosecond radiation, which consists of many focal spots corresponding to individual time slices of the pulse. The time slices located in the leading edge of the pulse have the minimum radius $R_{\mathrm{eff}\,t\mathrm{f}}$ at the focal point $z = z_{\mathrm{f}\,t}$, while the slices located in the trailing edge have the maximal radius (Fig. 3).

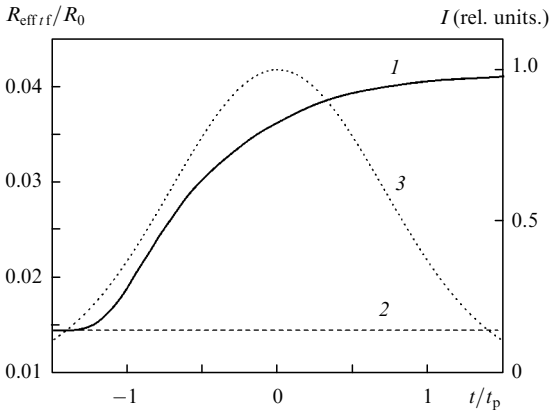

Figure 3. Effective radius $R_{\mathrm{eff}\,t\mathrm{f}}$ of the focal waist of each temporal slice as a function of the time position within the pulse (*1*), the waist radius upon linear focusing of radiation (*2*), and the temporal pulse profile (*3*).

The physical picture of the 'slice-by-slice' self-focusing of an ultrashort light pulse is in qualitative agreement with the dynamic moving focus (DMF) model proposed in [19, 20] and modified for ionised media and focused beams in [21, 22]. This model treats a light filament as a sequence of 'local' foci of different time slices of the pulse appearing at different distances from the optical path onset. The filament size at each point is equal to that of the corresponding focal spot. The DMF model predicts that the right boundary of a filament in the case of a preliminarily focused beam cannot come outside its geometrical focus [see expression (4)], which contradicts experiments and numerical calculations presented in Fig. 1.This discrepancy can be resolved by analysing the beam self-focusing in terms of effective parameters. Then, as follows from Fig. 2a, the minimum of the instant effective radius, restricting the spatial region of the instant power of each time slice of the pulse, is indeed always located to the left from the geometrical focus $z = z_{\mathrm{f}}$ of the beam. From this point of view, the DMF model does not contradict the physical picture of the effect under study and can be used for the qualitative interpretation of nonstationary focusing and tightly focused radiation.

The effective 'global' beam radius integrated over the entire pulse profile determines the size of the region where the greater part of the radiation energy is concentrated. Therefore, the dependence $R_{\mathrm{eff}}(z)$ almost completely repeats the dependence of the instant radius $R_{\mathrm{eff}\,t}(z)$ of the central part of the pulse [curves (*5*), (*6*), and (*10*) in Fig. 2a merge to one curve]. Note also that the growth rate of the effective

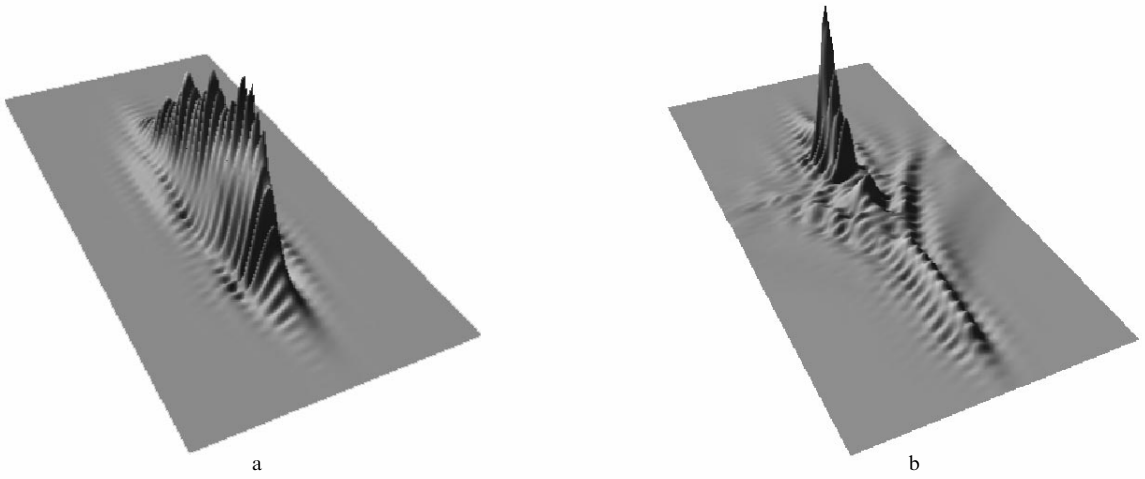

Figure 4. Spatiotemporal distribution of the relative intensity of a laser pulse $I(|\boldsymbol{r}_\perp|, z = z_{\mathrm{f}}, t)$ at the geometrical focus of the beam for initial radiation powers $\eta = 7$ (a) and 100 (b). The corrugated structure of the profiles is an artefact of the network approximation algorithm.

radius in each time slice behind the focal point along the path exceeds the transverse contraction rate in the slice and monotonically increases by the pulse end due to the increasing action of the plasma nonlinearity.

Figure 4 shows the spatiotemporal shape of the laser pulse in the form of the two-dimensional distribution of the normalised intensity $I(|\boldsymbol{r}_\perp|, z = z_f, t) = I/I_0 0$ of the wave at the focal point $z = z_f$ of the beam. The two distributions, corresponding to different initial pulse powers, are presented. One can see that the spatial intensity distribution changes drastically from the quasi-Gaussian distribution (Fig. 4a) to the arrow-like distribution (Fig. 4b) with increasing radiation power. In the latter case, the peak of the 'arrow' is directed towards the leading edge of the pulse (negative values of t), while the 'wings' are the result of radiation defocusing in the produced plasma region. Due to the radiation loss caused by photoionisation of air, the intensity maximum at the geometrical focal point at large η shifts from the pulse centre to its trailing edge (positive values of t).

Note that upon the self-action of a collimated femtosecond beam, unlike tightly focused radiation considered here, the light pulse has a different spatiotemporal structure in the nonlinear focal region. This structure exhibits, as a rule, the two main intensity maxima located in the leading and trailing edges of the pulse [23, 24]. This is explained by the fact that the dominating physical mechanism of the spatiotemporal compression of a collimated beam is the Kerr self-focusing, whereas the spatiotemporal compression of a tightly focused beam occurs due to linear focusing. As a result, the intensity of a collimated Gaussian beam increases more strongly on the beam axis, thereby considerably sharpening the transverse profile of the beam. In this region, the maximum energy loss occurs during the plasma production, which leads to the pulse segmentation along the time coordinate and the formation of a bimodal structure. The femtosecond pulse, compressing due to initial tight focusing, preserves its profile almost completely until the appearance of plasma, and no sharp time gradient is formed. In this case, the Kerr effect only 'helps' in linear focusing and its influence becomes noticeable only in the vicinity of the nonlinear focus. Therefore, in this case, the plasma formation in the medium will be provided both by the central part of the pulse and its leading edge. The trailing edge of the pulse propagates in a strongly absorbing medium, which has been ionised by the previous parts of the pulse and has the defocusing effect on optical radiation. This restricts a further increase in the pulse intensity due to the Kerr effect and linear focusing of radiation.

It is the influence of the initial focusing of radiation that also explains the fact that the temporal compression of a femtosecond laser pulse appearing during its self-focusing, which was pointed out in many theoretical papers (see, for example, review [13]), is less pronounced for tightly focused radiation compared to a collimated beam. It should be emphasised that this effect is most pronounced only near the light beam axis, in the region of the absolute maximum of the field intensity and correspondingly of the maximum influence of the Kerr nonlinearity of the medium. At the beam periphery during self-focusing, as follows from our studies [25], the time profile virtually does not change even for a collimated beam.

It is interesting to determine the maximal achievable intensity in the focal waist of a femtosecond laser pulse

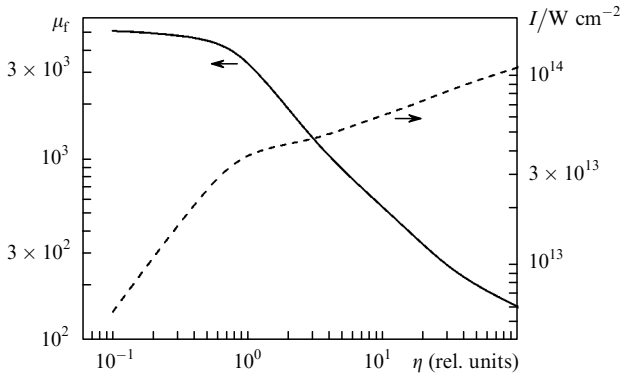

Figure 5. Dependences of the intensity μ_f in the focal waist of a femtosecond beam and of the maximum achievable intensity I_f on the initial radiation power.

depending on its power. According to (3), for the conditions of the numerical experiment upon linear focusing of a beam of radius $\bar{F}_0 = 0.028$, the calculated increase in the radiation intensity is $\mu_f = 5102$. As follows from the dependence presented in Fig. 5, such a value of the relative intensity is achieved only in the case of a strongly subcritical pulse power ($\eta \leqslant 0.1$). As the initial radiation power is increased, the parameter μ_f slowly decreases at moderate powers ($\eta = 0.5 - 1$) and then the relative radiation intensity in the focus decreases linearly with increasing η.

The coordinate z^* of a point of the path where the pulse intensity achieves a maximum is shown in Fig. 6. One can see that, upon focusing the subcritical-power radiation, the position of the pulse maximum exactly corresponds to the centre $z_f = 85.9$ cm of a linear focal waist. As the pulse power further increases, the point corresponding to the maximum intensity approaches the path onset, the approximate equality $z^* \simeq z_g$ being always fulfilled. In other words, upon focusing femtosecond radiation, the maximum radiation intensity is achieved near the 'global' focus of the beam, rather than the 'local' focus. The local focus position z_n determines only the beginning of a light filament.

Consider maximum radiation intensities achieved at the focus of the beam (dashed curve in Fig. 5). The break in the dependence $I_f(\eta)$, which is distinctly observed in Fig. 4, corresponds to the change of beam focusing regimes taking place when the radiation intensity I_f in the focus achieves

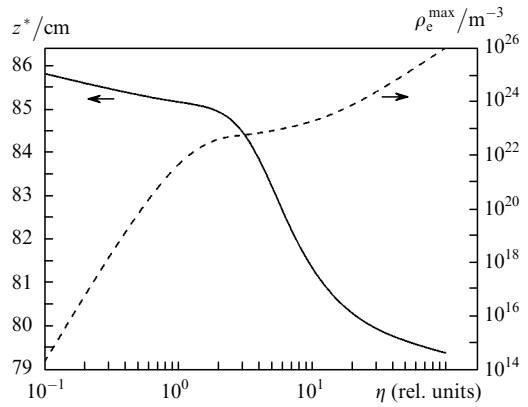

Figure 6. Coordinate z^* of the 'global' intensity maximum and the maximum free electron density ρ_e^{max} as functions of the initial radiation power.

$(2-4)\times 10^{13}$ W cm^{-2}. In the latter case, as pointed out above, the plasma nonlinearity begins to prevent noticeably (through a change in the refractive index of the medium) a further increase in the beam intensity occurring during the Kerr self-focusing of the beam. The competition of these two processes restricts the peak amplitude of the light wave in each temporal 'slice' of the pulse. Note that while the restriction of the peak intensity in the leading edge of the pulse is caused by the wave energy loss for gas photoionisation (the imaginary part of m_p), at the pulse centre and its trailing edge, refraction in the already produced plasma dominates (the real part of m_p). As follows from calculations (dashed curve in Fig. 6), the maximum free electron density ρ_e^{max} in the beam at which focusing regimes are changed is $\sim 10^{23}$ m^{-3}.

For the essentially supercritical beam power ($\eta \gg 1$), the continuing growth of the peak intensity in the nonlinear focus leads to the increase in the plasma density up to $\sim 10^{26}$ m^{-3}, which is already close to the equilibrium concentration of neutral nitrogen molecules in air (according to the calculation conditions, $\rho_{nt} \sim 1.2\times 10^{26}$ m^{-3}). This demonstrates a high, close to unity, photoionisation degree of the medium, as well as the possibility of the development of the electron avalanche and optical breakdown of air (the atmospheric air breakdown threshold is $\sim 2\times 10^{14}$ W cm^{-2} [10]). A further increase in the initial radiation power will no longer be efficient for increasing the peak intensity in the 'global' focus of the beam because the optical-breakdown plasma produced in the leading edge of the pulse will prevent the propagation of the remaining part of the pulse.

Let us introduce another effective parameter characterising the propagation of ultrashort light pulses – the effective intensity

$$I_{eff}(z) = \frac{E(z)}{\pi^{3/2} t_{eff\,p}(z) R_{eff}^2(z)},$$

where

$$t_{eff\,p} = \left[E^{-1}(z)\iint_{S_\perp} d^2\boldsymbol{r}_\perp \int_{-\infty}^{\infty} dt' I(\boldsymbol{r}_\perp, z, t') t'^2\right]^{1/2}$$

is the effective average pulse duration. According to this definition, the effective radiation intensity $I_{eff}(z)$ of a Gaussian pulse at each point of the path in a linear medium is equal to the peak value of the real intensity. Figure 7 demonstrates the dependences of the ratio $\mu_{eff} = I_{eff}(z)/I_0$ on the propagation length for focused beams with different initial powers. One can see that the nonstationary self-action of radiation changes the focusing dynamics of the beam, resulting in the displacement of its 'global' focal waist towards the radiation propagation direction and in a decrease in the average intensity maximum in the 'global' focus of the beam.

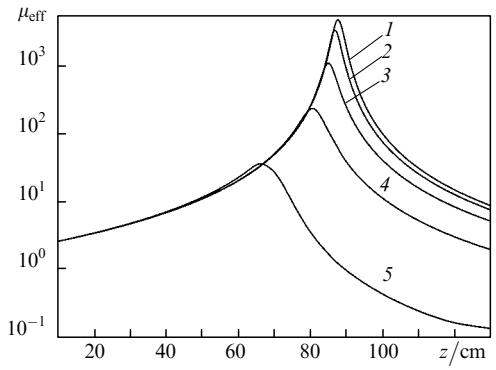

Figure 7. Dependences of the relative effective laser radiation intensity μ_{eff} on the propagation length z for initial pulse powers $\eta = 0.1$ (*1*), 1 (*2*), 3 (*3*), 125 (*4*), and 1009 (*5*).

Figure 8 shows the dependence of the effective radius $R_{eff\,f} = R_{eff}(z = z_g)$ of the beam focal waist on the initial power of focused femtosecond pulses. One can see that in the nonlinear propagation regime it is impossible to focus radiation into a diffraction-limited spot predicted by the linear theory [see expression (2)].

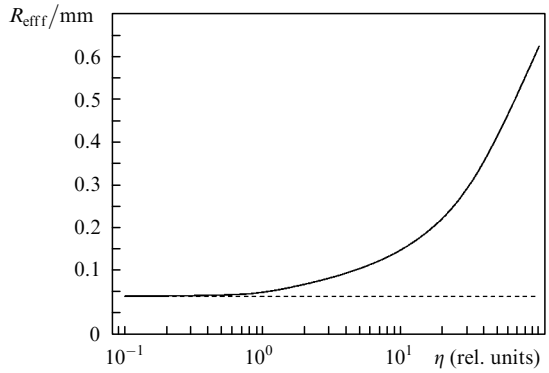

Figure 8. Effective radius $R_{eff\,f}$ of the focal waist of a femtosecond beam as a function of the initial radiation power η. The dashed straight line is the radius value during linear propagation.

It should be emphasised that we are dealing here with the effective integrated size of the focal beam waist (12), calculated as the focal radius of each temporal slice of the pulse averaged over the temporal power profile. This radius characterises the size of a region where the pulse energy is concentrated and it can differ from the instant radius of the beam determined from the intensity profile and having, as pointed out above (see Fig. 3), the minimal diffraction-limited value in the low-intensity region at the leading edge of the pulse. This can probably explain the extremely small focal spot size (diameter 2–3 μm) achieved in paper [5] upon focusing femtosecond pulses from a Ti : sapphire laser in air. Based on the results obtained above, we can conclude that the diffraction-limited (minimal) effective transverse size of the focal waist of a high-power ultrashort pulse can be obtained only at the leading edge of the pulse, i.e. where the plasma density is still not high and, therefore, the defocusing of radiation in the plasma is not strong yet.

6. Conclusions

Thus, numerical simulations of the propagation of tightly focused high-power ultrashort laser pulses in air have shown that the spatial shape and size of the focal beam waist (both in the longitudinal and transverse directions) depend on the initial pulse power. The spatial focusing of a laser ultrashort pulse of even subcritical power (for the Kerr self-focusing) can lead to the photoionisation of the

medium and plasma production in the region of the maximum beam intensity, which will restrict a further increase in the light-wave intensity and the transverse compression of the beam as a whole. The higher the radiation pulse intensity, the more complicated the spatial structure of the focal waist, which is transformed from a point spot to an extended axial filament of variable diameter consisting of many focal spots corresponding to individual temporal slices of the pulse.

The evolution of the effective radius of the laser beam along the optical path is similar to the behaviour of linearly focused radiation forming a distinct waist at the 'global' focal point. The difference of the regime of nonstationary focusing of a high-power pulse consists in the change in the divergence of radiation propagating through the 'global' focus and in the increase in the transverse size of the waist with increasing pulse power.

The rate of the increase in the maximum intensity of a focused light beam deceases with increasing the pulse power. From the point of view of achieving extremely high peak intensities (or power densities) at the 'global' focus of the beam, an increase in the initial radiation power is inefficient because the optical-breakdown plasma produced at the leading edge of the pulse will block the focusing of the next temporal slices of the pulse.

References

1. Schaffer C.B., Brodeur A., Garca J.F., Mazur E. *Opt. Lett.*, **26**, 93 (2001).
2. König K., Riemann I., Fischer P., Halbhuber K. *Cell. Mol. Biol.*, **45**, 192 (1999).
3. Zipfel W.R., Williams R.M., Christie R., Nikitin A.Y., Hyman B.T., Webb W.W. *Proc. of the National Academy of Science (PNAS)*, **100**, 7075 (2003).
4. Grimes M.K., Rundquist A.R., Lee J.-S., Downer M.C. *Phys. Rev. Lett.*, **82**, 4010 (1999).
5. Bukin V.V., Vorob'ev N.S., Garnov S.V., Konov V.I., Lozovoi V.I., Malyutin A.A., Shchelev M.Ya., Yatskovskii I.S. *Kvantovaya Elektron.*, **36**, 638 (2006) [*Quantum Electron.*, **36**, 638 (2006)].
6. Zemlyanov A.A., Geints Yu.E. *Opt. Atmos. Okean.*, **18**, 574 (2005).
7. Born M., Wolf E. *Principles of Optics* (Oxford: Pergamon Press, 1969; Moscow: Nauka, 1973).
8. Vlasov S.N., Talanov V.I. *Samofokusirovka voln* (Wave Self-focusing) (Nizhnii Novgorod, Institute of Applied Physics, RAS, 1997).
9. Turitsyn S.K., Mezentsev V.K., Dubov M., Rubenchik A.M., Fedoruk M.P., Podivilov E.V. *Opt. Express*, **15**, 14750 (2007).
10. Raizer Yu.P. *Fizika gazovogo razryada* (Gas Discharge Physics) (Moscow: Nauka, 1987).
11. Gol'dberg V.N., Talanov V.I., Erm R.E. *Izv. Vyssh. Uchebn. Zaved., Ser. Radiofiz.*, **10**, 674 (1967).
12. Akozbek N., Bowden C.M., Talebpour A., Chin S.L. *Phys. Rev. E*, **61**, 4540 (2000).
13. Berge L., Skupin S., Nuter R., Kasparian J., Wolf J.-P. *Rep. Prog. Phys.*, **70**, 1633 (2007).
14. Kandidov V.P., Kosareva O.G., Mozhaev E.I., Tamarov M.P. *Opt. Atmos. Okean.*, **13**, 429 (2000).
15. Zemlyanov A.A., Geints Yu.E. *Opt. Atmos. Okean.*, **20**, 40 (2007).
16. Perelomov A.M., Popov V.S., Terent'ev M.V. *Zh. Eksp. Teor. Fiz.*, **50**, 1393 (1966).
17. Talebpour A., Yang J., Chin S.L. *Opt. Comm.*, **163**, 29 (1999).
18. Bagaev S.N., Geints Yu.E., Zemlyanov A.A., Kabanov A.M., Matvienko G.G., Pestryakov E.V., Stepanov A.N., Trunov V.I. *Opt. Atmos. Okean.*, **20**, 413 (2007).
19. Lugovoi V.M., Prokhorov A.M. *Pis'ma Zh. Eksp. Teor. Fiz.*, **7**, 153 (1968).
20. Lou M.M.T., Shen Y.R. *Phys. Rev. Lett.*, **22**, 994 (1969).
21. Brodeur A., Kosareva O.G., Chien C.Y., Ilkov F.A., Kandidov V.P., Chin S.L. *Opt. Lett.*, **22**, 304 (1997).
22. Lange H.R., Grillon G., Ripoche J.-F., Franco M.A., Lamouroux B., Prade B.S., Mysyrowicz A., Nibbering E.T.J., Chiron A. *Opt. Lett.*, **23**, 120 (1998).
23. Golubtsov I.S., Kandidov V.P., Kosareva O.G. *Opt. Atmos. Okean.*, **14**, 335 (2001).
24. Sukhorukov A.P., Vislobokov N.Yu. *Kvantovaya Elektron.*, **37**, 1015 (2007) [*Quantum Electron.*, **37**, 1015 (2007)].
25. Zemlyanov A.A., Geints Yu.E. *Eur. Phys. J. D*, **42**, 349 (2007).